Supporting On-Line Material for: Revealing Sub-Surface Vibrational Modes by Atom-Resolved Damping Force Spectroscopy

Makoto Ashino, Roland Wiesendanger, Andrei N. Khlobystov, Savas Berber, and David Tománek

PACS numbers: 81.05.Tp, 61.48.De, 68.37.Ps 68.35.Ja

SAMPLE PREPARATION

Synthesis and deposition of ($Dy@C_{82}$)@SWNT peapods on a Si/SiO_2 substrate

Single-walled carbon nanotubes (SWNTs) were synthesized by arc discharge using a non-magnetic catalyst [1] and heated in air at 440°C for 30 minutes to open their ends. The nanotube diameters were determined by measuring the Radial Breathing Mode (RBM) frequency using Raman spectroscopy. On top a broad distribution of RBM frequencies, we found discrete peaks indicating abundance of nanotubes with diameters $12.6-13.0$ Å, $14.8-15.0$ Å, $16.2-16.8$ Å, and $18.1-18.4$ Å. $Dy@C_{82}$ endohedral metallofullerenes were produced by arc vaporization and purified by high-performance liquid chromatography. The $Dy@C_{82}$ molecules were encapsulated into the SWNTs with different diameters by heating their mixture in a platinum crucible under 10^{-6} Torr at 440°C for 5 days [2].

High-resolution transmission electron microscopy (HRTEM) was used to verify the presence of $Dy@C_{82}$ inside the nanotubes, showing the fullerene cages as circles and the enclosed Dy atoms as dark spots positioned off the center. According to extensive HRTEM observations, the proportion of filled nanotubes was ≈60%. The mixture of SWNTs and ($Dy@C_{82}$)@SWNT peapods was dispersed in a 1% aqueous SDS solution and deposited onto a highly doped Si substrate covered by a 0.2 μm thick layer of dry SiO_2 [2]. The samples were subsequently heated in ultrahigh vacuum at 150°C for 2 hours to remove the solvent and other adsorbed molecules.

METHODS

Principle of dynamic AFM

We used Atomic Force Microscopy (AFM) [3] as a primary tool to investigate the deposited nanotubes and peapods in real-space, independent of their electronic properties, by probing the interaction between a sharp AFM tip and the sample. In the dynamic operation mode, illustrated in Fig. 1, a cantilever mounted on a piezo actuator is oscillated at its eigenfrequency f_0 by a self-excitation resonance loop. Tip-sample interactions, involving long- and short-range terms, shift the eigenfrequency by $\Delta f = f - f_0$. Note that for the operation with relatively large oscillation amplitudes A compared to the range of tip−sample interactions, it is convenient to describe the "normalized frequency shift", defined as $\gamma = (c_z A^{3/2}/f_0)\Delta f$, where c_z is the cantilever spring constant [4]. We use a feedback control based on the frequency modulation technique [5] to maintain a constant value of Δf during the scan, which in turn yields the surface topography. By compensating long-range electrostatic and van der Waals interactions, it is possible to achieve true atomic resolution in surface topography

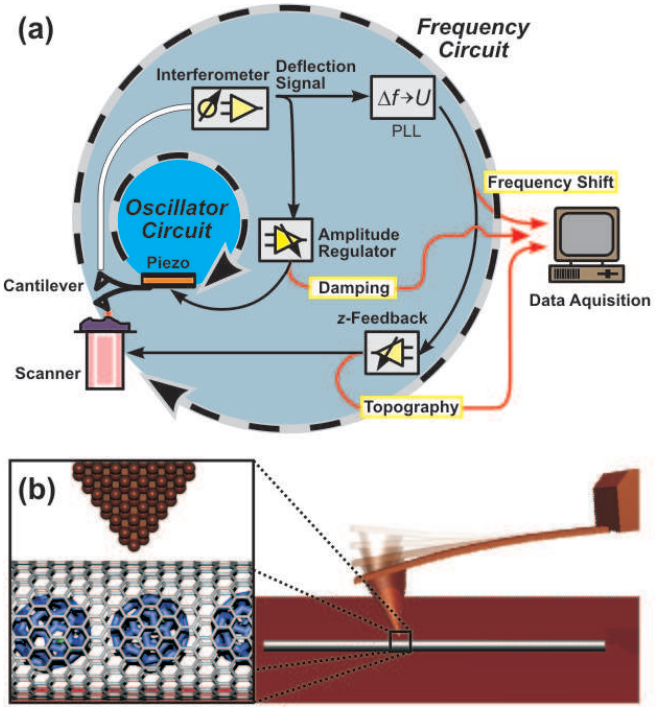

FIG. 1: (Color) (a) Schematic operational diagram of a dynamic Atomic Force Microscope (AFM) system. Using two separate feedback control channels, surface topography and energy loss ΔE images are acquired simultaneously. (b) Close-up picture (left) and overview picture (right) depict a sharp AFM tip, mounted on an oscillating silicon cantilever, as it probes the peapod. Interaction between the tip apex atom and the peapod shifts the resonance frequency and dampens the oscillation. Topography images are obtained by scanning the peapod under feedback control to keep the frequency shift Δf constant.

measurements [4]. Careful adjustment of the operating regime of the non-contact AFM with a sharp tip makes it possible to decouple atomically resolved topography features from effects caused by an elastic deformation of the sample [6].

AFM instrumentation

Our experiments were performed using a home-built low-temperature AFM operating in ultra-high vacuum and optimized for atomic-scale studies [7]. The AFM was operated at a background pressure of $p < 1\times10^{-8}$ Pa and a temperature $T < 13$ K. All results presented here were acquired using commercial silicon cantilevers (SSS-NCL, Nanosensors, Switzerland) with the spring constant $c_z = 34.3$ N/m and a sharp tip of monocrystalline Si with a nominal radius of 20 Å. After transfer into the vacuum, the probe tips were cleaned by argon ion sputtering. To compensate the effect of long-range electrostatic forces, we modified the average contact potential difference by applying bias voltage $U_{\rm bias}$ to the cantilever [8].

The sharpness and the effective shape of the tip were deduced by deconvoluting AFM images of SWNTs, used for calibration, with diameters ranging from 13.0±0.3 Å to 16.2±0.5 Å, depicted in Fig. 2(a:1) of the main article. We found the AFM tip to be 'atomically sharp', with the estimated tip apex radius $r_{\rm apex} < 5$ Å. We obtained images with atomic resolution and no 'ghost structures' (caused by double-tips), consistent with lattice parameters of graphitic carbon. We used an oscillation amplitude $A = 21 - 23$ Å in the dynamic AFM operation. In view of the high Young's moduli $Y = 180$ GPa [9] of the Si tip and the effective value of 17 GPa [10] for the radial deformation of the nanotube, elastic deformations associated with the tip-nanotube interaction were found to lie within the noise range for nominal forces below 250 pN. According to our estimates based on the spring constant and oscillation amplitude, the damping energy as well as the tip-substrate interaction were too small in the operating range of our experiment to cause problems such as jump-to-contact and other instabilities of the cantilevers, mostly related to the hysteresis depicted in Fig. 1(d) of the main article [4].

Detection of the damping signal ΔE

The feedback control, which maintains a constant amplitude A of the oscillating cantilever, also provides valuable information about spatial variations of the energy loss, which causes damping. This energy loss ΔE per cycle of the cantilever oscillation is given by [4]

$$\Delta E(x,y,z) = \pi \frac{c_z A^2}{Q_0} \left[\frac{G(x,y,z)}{G_0} - \frac{f(x,y,z)}{f_0} \right] . \quad (1)$$

Here, Q_0 is the intrinsic quality factor and G the gain factor, which maintain a constant oscillation amplitude. In the dynamic AFM operation, the non-conservative tip-sample interaction causing the hysteretic behavior in the approach-retraction cycle, illustrated in Fig. 1(d) of the main article, is the main mechanism for energy dissipation [11]. The quantity $\Delta E(x,y,z)$ is the signal probed by Damping Force Spectroscopy (DFS).

ACQUISITION AND INTERPRETATION OF DATA

Topography and damping data

In order to distinguish (Dy@C_{82})SWNT peapods from empty SWNTs on the basis of their image contrast, we prepared a reference sample by depositing 100% empty SWNTs on SiO_2. Images obtained on this reference sample were compared to a sample containing a mixture of empty SWNTs and filled nanotubes (peapods), which we used in our study. With no prior knowledge, which individual nanotube is filled and which is empty, we imaged several tens of nanotubes with the AFM. We considered

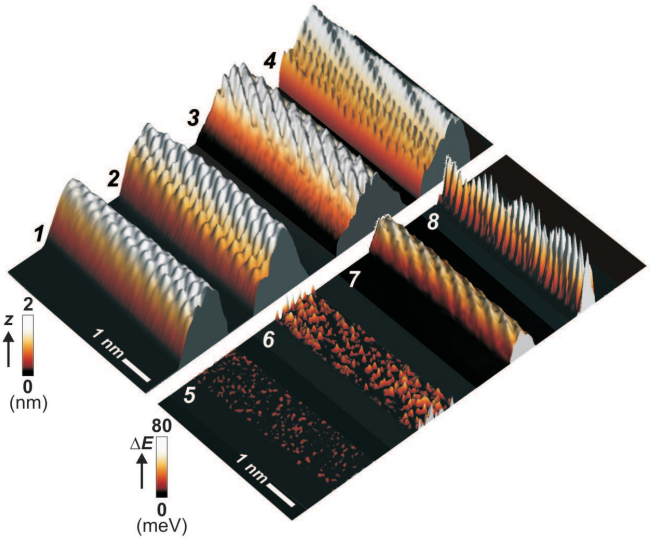

FIG. 2: (Color) Simultaneously observed dynamic AFM topography (1-4) and damping (5-8) signals of various nanotubes and peapods. The data and labelling of the panels are identical to Fig. 2(a) of the main article. The images represent an empty SWNT (1,5) with d = 16.2±0.5 Å and (Dy@C_{82})@SWNT peapods with diameters d = 16.2±0.3 Å (2,6), 15.0±0.5 Å (3,7), and 13.0±0.5 Å (4,8). The global imaging parameters were $c_z = 34.3$ N/m and $U_{\rm bias} = -300$ mV. For images (1,2,5,6) we used $f_0 = 159$ kHz, $\Delta f = -99.0$ Hz, $\gamma = -2.33$ fNm$^{1/2}$, and $A = 22.9$ Å. For images (3,7) we used $f_0 = 160$ kHz, $\Delta f = -63.8$ Hz, $\gamma = -1.42$ fNm$^{1/2}$, and $A = 21.7$ Å. For images (4,8) we used $f_0 = 159$ kHz, $\Delta f = -53.3$ Hz, $\gamma = -1.14$ fNm$^{1/2}$, and $A = 21.4$ Å.

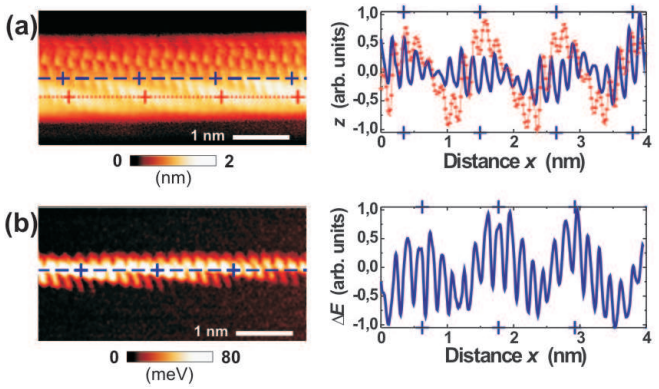

FIG. 3: (Color) Results of simultaneous (a) topographic AFM and (b) damping measurements of the nanotube peapod represented in panels (4,8) of Fig. 2. In the atomic-resolution images, local maxima reflect the atomic positions in the chiral enclosing nanotube and those of the enclosed metallofullerenes. The scan data are represented as color-coded 2D images in the left panels. Red- and blue-colored graphs in the right panels show original scan data along trajectories indicated by the same color and dashed or dotted pattern in the left panels.

an axial undulation in the topography and a damping signal with the period of $10-11$ Å, and the presence of significant damping as primary evidence of dealing with a peapod. We found our AFM-based distinction between peapods and unfilled nanotubes to be consistent with the HRTEM finding that about 60% nanotubes were filled.

Figure 2 displays simultaneously observed topography and damping signals for selected empty and filled SWNTs. The simulated 3D images offer a different perspective than the 2D view shown in Fig. 2(a) of the main article. The data were obtained using an atomically sharp tip at temperatures close to 13 K. The samples were scanned at a very low speed of $16-24$ Å/s, while the frequency shift Δf has been kept constant using a feedback control. The scan direction was horizontal, i.e. parallel to the tube axis, in all images to prevent tip-induced nanotube displacement. We found AFM topography images of empty SWNTs, such as that in Fig. 2(1), to be symmetric with respect to the axis, which indicate that the tip shape should be symmetric. Some degree of asymmetry, on the other hand, was observed in panels 2-4 of Fig. 2, displaying topography images of peapods. Possible causes of this lateral asymmetry could be either a genuine Dy@C_{82} metallofullerenes within the peapod (which may be spontaneous or induced by the AFM), or an artifact of the measurement. We find it conceivable that an ordered subsurface structure, in particular an off-axis location of the encapsulated metallofullerenes in wide nanotubes, could cause a lateral asymmetry in the AFM signal. In that case, the net charge on the Dy ion and the enclosing fullerene may cause an electric field with a non-axially symmetric distribution outside the peapod, which would exert an extra force on the tip.

Even though extra precautions have been taken to avoid artifacts caused by tip-induced lateral displacement of the nanotube (we scanned in the axial direction) and feedback lag (our scan speed is small), we can not exclude artifacts caused by tip asymmetry as the origin of the observed lateral asymmetry in topographic images of peapods. Since we use heavily doped Si cantilevers, an asymmetric doping profile may evolve also on the Si tip with an otherwise symmetric morphology. Should this indeed be the case, an asymmetry in the charge distribution on the tip should not be noticeable when probing locally charge neutral SWNTs, but could play a more important role when probing (Dy@C_{82})@SWNT peapods with a significant charge re-distribution.

In Fig. 3 we present a detailed comparison between topography and damping observations for the same peapod. Besides color-coded 2D images, we also plot the raw data for individual scan lines. The profiles in the right panels of Fig. 3, where the vertical scales are normalized, show that the atomic-scale contrast in damping (bottom panels) is generally larger than in topography (top panels). Positions of relative maxima in topography and damping along the same blue-dashed trajectory are indicated by the blue crosses. Our results indicate that the position of relative maxima in damping lies consistently $2-3$ Å to the right of the maxima in topography. The axial band with maximum contrast in damping, shown in the left panel of Fig. 3(b), is much narrower and positioned differently from the band of maximum contrast in topography, indicated in Fig. 3(a) by the red dotted trajectory. We believe that this is one more indication that the damping signal is a source of new, rich information surpassing that of pure topography measurements.

Molecular dynamics simulations

Our molecular dynamics (MD) simulations analyze the atomic motion in a peapod following an initial perturbation. In each simulation, we consider one isolated $(n,0)$ nanotube, with $n=17-21$, filled with C_{82} fullerenes. We use periodic boundary conditions along the tube axis and 52.6 Å long unit cells containing four fullerenes to suppress artifacts introduced by the periodic boundary conditions. The tip-induced perturbation is modelled by radially displacing ("plucking") one atom on the nanotube outward by 0.3 Å and abruptly releasing it. Microcanonical MD simulations with a time step of 0.5 fs monitor the motion of all atoms for a time period of 50 ps. MD runs for different tube diameters and relative position of the plucked atom with respect to the underlying fullerenes are analyzed by monitoring the radial motion $\Delta r(t)$ of the plucked atom and the radial center of mass motion $\Delta r_{CM}(t)$ of the enclosed fullerenes. Fourier analysis of $\Delta r(t)$ and $\Delta r_{CM}(t)$ provides information about

the modes that accommodate and dissipate the energy provided by the tip in non-contact regime.

[1] M. Haluška, M. Hulman, B. Hornbostel, J. Čech, V. Skákalová, and S. Roth, Phys. Stat. Sol. (b) **243**, 3042 (2006).

[2] D. Obergfell, J. C. Meyer, M. Haluška, A. N. Khlobystov, S. Yang, L. Fan, D. Liu, and S. Roth, Phys. Stat. Sol. (b) **243**, 3430 (2006).

[3] G. Binnig, C. F. Quate, and C. Gerber, Phys. Rev. Lett. **56**, 930 (1986).

[4] S. Morita, R. Wiesendanger, and E. Meyer, *Noncontact Atomic Force Microscopy*, NanoScience and Technology (Springer, Berlin, 2002).

[5] T. R. Albrecht, P. Grütter, D. Horne, and D. Rugar, J. Appl. Phys. **69**, 668 (1991).

[6] M. Ashino, D. Obergfell, M. Haluška, S. Yang, A. N. Khlobystov, S. Roth, and R. Wiesendanger, Nature Nanotech. **3**, 337 (2008).

[7] W. Allers, A. Schwarz, U. D. Schwarz, and R. Wiesendanger, Rev. Sci. Instrum. **69**, 221 (1998).

[8] M. Ashino, A. Schwarz, T. Behnke, and R. Wiesendanger, Phys. Rev. Lett. **93**, 136101 (2004).

[9] M.-F. Yu, T. Kowalewski, and R. S. Ruoff, Phys. Rev. Lett. **85**, 1456 (2000).

[10] L. Shen and J. Li, Phys. Rev. B **69**, 045414 (2004).

[11] L. N. Kantorovich and T. Trevethan, Phys. Rev. Lett. **93**, 236102 (2004).